The Astrophysical Journal, 771:47 (11pp), 2013 July 1 doi:10.1088/0004-637X/771/1/47

EXPLORATION OF A RELIC CIRCUMSTELLAR ENVELOPE IN THE "WATER FOUNTAIN" SOURCE IRAS 18286−0959

Hiroshi Imai[1,2], Jun-ichi Nakashima[3], Bosco H. K. Yung[3], Shuji Deguchi[4], Sun Kwok[3], and Philip J. Diamond[5]
[1] Department of Physics and Astronomy, Graduate School of Science and Engineering, Kagoshima University, 1-21-35 Korimoto, Kagoshima 890-0065, Japan; hiroimai@sci.kagoshima-u.ac.jp
[2] International Centre for Radio Astronomy Research, M468, The University of Western Australia, 35 Stirling Hwy, Crawley, Western Australia 6009, Australia
[3] Department of Physics, University of Hong Kong, Pokfulam Road, Hong Kong, China; junichi@hku.hk, byung@hku.hk, sunkwok@hku.hk
[4] Nobeyama Radio Observatory, National Astronomical Observatory of Japan, Minamimaki, Minamisaku, Nagano 384-1305, Japan; deguchishuji60@gmail.com
[5] SKA Organisation, Jodrell Bank Observatory, Lower Withington, Macclesfield, Cheshire SK11 9DL, UK; diamond@skatelescope.org
Received 2013 January 11; accepted 2013 May 4; published 2013 June 14

ABSTRACT

The *water fountain* source IRAS 18286−0959 (I18286) was reported as an object exhibiting highly collimated, double-helix stellar jets traced by the H_2O maser emission. Using the European VLBI Network, we measured the absolute coordinates of the 1612 MHz OH maser emission in I18286, which is very likely associated with a relic of a circumstellar envelope (CSE) developed in the asymptotic giant branch stage of the central star. The location of the OH maser is near the center of the H_2O maser feature cluster, where one of the originating points of the two jets is located. We also mapped 22.2 GHz H_2O maser emission in this object using the Very Long Baseline Array in the seasons of 2006–2007 as well as 2008–2009. In the first three epochs in 2006–2007, we detected at least 90 maser features per epoch. In six epochs in 2008–2009, when the observation data had already been published and analyzed to identify the double-helix jets, we newly identified 14 proper motions of H_2O maser features which could not be measured in the previous analysis due to their short lifetimes. In this paper, together with the OH maser emission, we focus on "outlier" H_2O maser features, which exhibit slow expansion velocities ($V_{\rm exp} \lesssim 30$ km s^{-1}) and are likely associated with either the relic CSE or an *equatorial flow* of I18286. They were marginally distinguishable from the maser features associated with the jets in I18286.

Key words: masers – stars: AGB and post-AGB – stars: individual (IRAS 18286−0959) – stars: mass-loss – stars: winds, outflows

Online-only material: machine-readable table

1. INTRODUCTION

A stellar jet seen at the final stage of stellar evolution is a manifestation of the important but still poorly understood phenomenon followed by formation of asymmetric planetary nebulae (PNe). In fact, bipolar and multipolar morphologies are frequently found in a sample of young PNe in optical and radio images. It has been expected that such a stellar jet is a major factor shaping these objects (e.g., Sahai & Trauger 1998). Similar morphologies have been found in the earlier phase, so-called pre-planetary nebulae (PPNe; Sahai 2004; Sahai et al. 2007). This fact leads to the current paradigm that such a collimated jet is launched at the earlier phase of stellar evolution—the asymptotic giant branch (AGB) phase—or soon after the AGB phase (the post-AGB phase; e.g., Vinković et al. 2004).

There are a small number of candidate sources that show us the earliest stage of stellar jet emergence. "Water fountain" sources are the most promising candidates; they are stellar objects that have extremely high-velocity flows traced by H_2O maser emission. The outflow velocity often exceeds a typical value of expansion velocities of circumstellar envelopes (CSEs) of Mira variable and OH/IR stars, which are observable in a double-peaked spectrum of 1612 MHz OH maser emission (10–25 km s^{-1}, e.g., te Lintel Hekkert et al. 1989). There are 15 water fountains that have been identified to date (Imai 2007; Desmurs et al. 2012). Very long baseline interferometry (VLBI) observations of some of these H_2O maser sources have revealed that the jets are highly collimated and they have extremely short dynamical timescales ($\lesssim$100 yr; Imai et al. 2002, 2007; Boboltz & Marvel 2005; Imai 2007; Claussen et al. 2009; Day et al. 2010; Yung et al. 2011, hereafter Paper I). The results of polarimetry of H_2O and OH masers associated with the water fountain sources suggest that the stellar magnetic field plays an important role in the launch and collimation of the jet (e.g., Vlemmings et al. 2006; Amiri et al. 2010, 2011). Interestingly, some of the water fountains exhibit precession of the jet (Imai et al. 2005; Paper I). The point-symmetric placement of the H_2O maser spot clusters is also often observed with respect to the originating point of the jet. Similar point-symmetric structures have been seen in optical images of many PNe and pre-PNe. It suggests that jet-induced shock structures are both spatially and dynamically centered on the star. Because the H_2O maser emission in the water fountains is usually observed over 100 AU away from the central stellar objects, it does not directly reveal regions close to the central stars. In addition, it is still unclear what the dynamical center of the jet coincides with, the evolved star itself or any others. Nevertheless, the observed properties of the H_2O masers mentioned above very likely provide important clues to identifying the central engines of the jets (either a single star or a binary system).

Here, note that a molecular jet traced by H_2O maser emission will disappear within 1000 yr or less because of the forthcoming photodissociation of H_2O molecules by the central objects of PNe. In fact, H_2O masers observed in PNe do not exhibit bipolar fast jets, while bipolar lobes are found in the radio continuum emission of the same PNe (Miranda et al. 2001; de Gregorio-Monsalvo et al. 2004). Recently, high-velocity H_2O masers were observed in a PN candidate as well (Suárez et al. 2009, 2012), while the dynamical timescale of the maser

region is longer than those confirmed in VLBI observations as mentioned above. However, taking into account requirement of the gas to be in a molecular form before photodissociation and ionization, one can infer that these masers are not associated with ionized jets themselves or these objects are not fully ionized PNe as suggested from optical observations. Because the bipolar structures of H_2O masers observed in these objects seem to be kept in those of the radio continuum emission in PNe (or PN candidates), it may be concluded that the fundamental structure of the stellar jet has been developed in the water fountain phase before photoionization emerges.

On the other hand, in a rapid evolution during the aforementioned timescale, *relic* AGB CSEs are still observable in 1612 MHz and H_2O maser emission in some water fountains. Interestingly, the expansion velocities of the water fountain relic CSEs cover a larger velocity range, considerably over the typical value of the aforementioned AGB CSEs (Imai et al. 2008; Claussen et al. 2009). It is unclear whether such a relic CSE is just a final form of the typical AGB CSE (e.g., Lewis 2001), or a by-product of the newly formed jet, so-called an *equatorial* flow. The latter, which is still somewhat hypothetical, is supported by possible correlation of the dynamical timescale of the jet with that of the torus seen in a PPN (Huggins 2007). Some H_2O maser features in the water fountain sources have kinematically large deviations from the collimated jets. Such a small number of "outlier" H_2O maser features may be another agent to characterize the evolution of the water fountains, providing a clue to understanding coevolution of the jet and the torus (or equatorial flow) (Huggins 2007). Thus the spatiokinematical structures of the H_2O maser emission should undergo substantial evolution, which might be directly confirmed by long-term observations followed by next-generation astronomers.

In this paper, we present the case of IRAS 18286−0959 (hereafter abbreviated as I18286). The location of the 1612 MHz OH maser emission was measured using the European VLBI Network (EVN), whose preliminary result was reported in Imai et al. (2008). The spatiokinematical structure of the old CSE and its relation to that of the H_2O masers is described in this paper in more detail. One can suppose that the presence of this maser emission directly indicates the existence of a persistent CSE in I18286.

The spatiokinematics of H_2O masers in I18286 was revealed using the Very Long Baseline Array (VLBA) data. This preliminary result was reported in Imai (2007). Paper I has already presented the spatiokinematical structure of H_2O masers in I18286 using the same data of VLBA and proposed a collimated, precessing, double-helix jet model for the H_2O masers as mentioned above. In this paper, we mainly focus the subject on the "outlier" H_2O masers, which are likely associated with a different kinematical component from the double-helix jets modeled in Paper I. Note that the position-reference maser feature for the maser proper-motion measurement in Paper I was one of such outlier H_2O masers discussed in this paper. Imai et al. (2013b, hereafter Paper II) determined the trigonometric parallax distance to I18286 to be $D = 3.61^{+0.63}_{-0.47}$ kpc. The distance to I18286 of 3.6 kpc is adopted in this paper. It is noteworthy that some of masers including the one used for the trigonometric parallax measurement (IRAS 18286−0959:I2013 *14* in Paper II) are clearly distinguishable spatially and kinematically from those associated with the modeled jets.

Section 2 describes in detail the VLBA observations of the H_2O masers in I18286 (Section 2.1) and the EVN observation of the OH maser (Section 2.2). Section 3 shows the whole spatiokinematical structures of the H_2O masers in I18286 (Section 3.1) and the location of the OH maser emission in the distribution of the H_2O masers (Section 3.2). In Section 3.3, we discuss the main issue of this paper: what the "outlier" H_2O masers are associated with, a newly developed equatorial flow or just a relic AGB CSE.

Table 1
Parameters of the VLBA Observations and Data Reduction for Individual Epochs

Code	Epoch (yy/mm/dd)	V_{ref} [a]	Noise[b]	Beam[c] (mas)	N_f[d]
BI033A	06/09/15	11.8	2.7	1.99 × 1.12, 25.°9	114
BI033B	06/11/09	79.2	1.0	2.31 × 1.33, 22.°5	141
BI033C	07/02/03	82.4	1.1	1.81 × 1.05, −1.°5	90

Notes.
[a] LSR velocity at the phase-reference spectral channel in units of km s^{-1}.
[b] rms noise in units of mJy $beam^{-1}$ in the emission-free spectral channel image.
[c] Synthesized beam size resulting from natural weighted visibilities, major and minor axis lengths, and position angle.
[d] Number of the detected maser features.

2. OBSERVATIONS AND DATA REDUCTION

2.1. VLBA Observations

The VLBA observations of the I18286 H_2O ($J_{K_-K_+} = 6_{12} \rightarrow 5_{23}$ at 22.235080 GHz) masers were conducted three times during 2006 September–2007 February (project code BI033) and six times during 2008 April–2009 May (BI037). Because the results of the latter season have already been published in Paper I, the details of the observations are not presented here. In this paper, we used the same H_2O maser positions as those in Paper I for further analysis (see Sections 3.1 and 3.3). Table 1 summarizes the status of the VLBA observations and data reduction in the former season. In the observations in the same season, another H_2O maser source IRAS 18460−0151 was also observed at the same observation session (Imai et al. 2013a), so the on-source time for I18286 was limited to 3 hr. A continuum source OT 081 was also observed for 4 minutes in every 20 minutes for calibration of group-delay residuals and bandpass characteristics. The received signals were recorded at a rate of 128 Mbits s^{-1} in 2 bits quantization into eight baseband channels (BBCs) in dual circular polarization. The centers of four pairs of BBCs, each of which had a bandwidth of 4 MHz, were set to velocities of −26.5, 27.0, 80.5, and 134.0 km s^{-1} with respect to the local standard of rest (LSR). The recorded data were correlated with the Socorro FX correlator using an integration period of 2 s. The data of each BBC were divided into 256 spectral channels, corresponding to a velocity spacing of 0.21 km s^{-1} per spectral channel. The following coordinates of I18286 were adopted as the delay-tracking center in the data correlation: $\alpha_{J2000} = 18^h31^m22^s.93$, $\delta_{J2000} = -09°57'19''.5$.

For the data reduction, we used the NRAO's AIPS package and adopted a normal procedure. After calibration of group-delay residuals and bandpass characteristics using scans on OT 081, fringe fitting and self-calibration were made using a spectral channel that contained bright maser emission. The LSR velocity of the spectral channel selected as phase and position reference is given in Column 3 of Table 1. The obtained solutions of calibration were applied to the data in all spectral channels. Finally, image cubes of the maser source

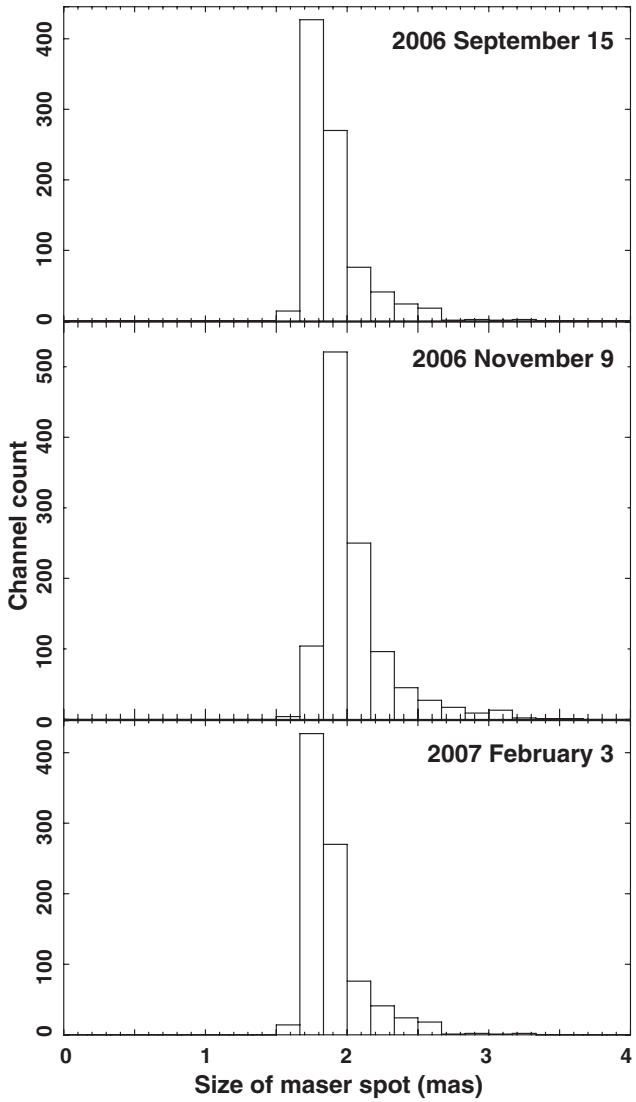

Figure 1. Histogram of sizes of H_2O maser spots in IRAS 18286−0959.

were obtained in visibility deconvolution through the CLEAN algorithm. In the image synthesis, we used visibilities that yielded good self-calibration solutions, while such solutions were missing in longer VLBI baselines because H_2O maser spots (velocity components) were spatially resolved (see also Paper I). Thus, a typical synthesized beam was extended to 2.3 mas. Columns 4 and 5 in Table 1 give values of the 1σ noise level and the synthesized beam pattern, respectively. The detected maser spots were objectively identified as Gaussian brightness components using an AIPS POPS pipeline script. Figure 1 shows the histogram of the measured size of H_2O maser spot in I18286. We found that the obtained spot sizes are larger than those typically found in other H_2O maser sources located at distances of 3 kpc and more, which is consistent with the results of Paper II. It may be attributed to the proximity of I18286 to the Galactic midplane where stronger interstellar scattering is expected. We determined the position of a maser feature (a physical maser clump consisting of a cluster of maser spots or velocity components located at almost the same position and velocity) by estimating a peak of brightness among the spots in the feature (Imai et al. 2002). Table 2 lists all H_2O maser features detected in the observations.

Table 2
Parameters of the Detected H_2O Maser Features

V_{LSR}[a] (km s^{-1})	R.A. Offset[b] (mas)	Decl. Offset[b] (mas)	I[c] (Jy beam^{-1})	ΔV[d] (km s^{-1})
		2006 September 15		
159.71	39.37 ± 0.06	−205.98 ± 0.19	0.04	0.63
158.66	38.98 ± 0.13	−206.30 ± 0.11	0.03	0.11
158.03	39.63 ± 0.09	−206.03 ± 0.17	0.03	0.63
157.82	38.01 ± 0.13	−207.03 ± 0.10	0.03	0.84
155.52	38.31 ± 0.11	−207.07 ± 0.14	0.06	3.16
153.39	38.25 ± 0.13	−207.34 ± 0.15	0.05	2.32
150.70	38.24 ± 0.02	−207.39 ± 0.05	0.25	3.16
143.06	34.52 ± 0.08	−195.19 ± 0.08	0.03	0.42
142.29	30.89 ± 0.06	−198.73 ± 0.09	0.04	1.05
138.99	38.71 ± 0.03	−209.75 ± 0.05	0.13	1.69

Notes.
[a] Local-standard-of-rest velocity at the intensity peak.
[b] Position offset with respect to the maser spot in the phase-reference velocity channel.
[c] Peak intensity of the feature.
[d] Full velocity width of maser emission. The minimum is equal to the velocity spacing of a spectral channel (0.21 km s^{-1}).

(This table is available in its entirety in a machine-readable form in the online journal. A portion is shown here for guidance regarding its form and content.)

2.2. EVN Observations

The EVN observation of I18286 in the OH ($F_j = 1^+ \rightarrow 2^-$ $^2\Pi_{3/2}$ at 1.612231 GHz) line (project code EI009A) was conducted on 2007 June 10 using following telescopes: Lovell 70 m in Jodrell Bank, Cambridge 32 m, Westerbork Synthesis Radio Telescope (14 25-m), Medicina 32 m, Noto 32 m, Effelsberg 100 m, Onsala 25 m, Torun 32 m, and Hartebeesthoek 26 m. For astrometry of the maser source, we adopted the antenna-nodding phase-referencing technique (e.g., Beasley & Conway 1995). With all the telescopes except Lovell 70 m, I18286 and the phase-reference continuum emission source J183220.8−103511 (hereafter abbreviated as J1832) were scanned in a switching cycle period of 5 minutes, resulting in total duration of scans on I18286 to be ∼3 hr. On the other hand, Lovell 70 m observed only I18286 without the antenna nodding. With all the telescopes, J174358.8−035004 was also observed for 3 minutes every 40 minutes for calibration of group-delay residuals and bandpass characteristics. The received signals were recorded at a rate of 128 Mbits s^{-1} in 2 bits quantization into eight BBCs in dual circular polarization. One pair of BBCs had a bandwidth of 1 MHz and others had 4 MHz to observe the I18286 H_2O maser and the J1832 continuum emission, respectively. The recorded data were correlated with the Mark IV processor in the Joint Institute for VLBI in Europe using an integration period of 4 s. The data of each BBC were divided into 512 and 32 spectral channels, respectively, for the maser and continuum observations. A velocity channel spacing of 0.36 km s^{-1} was obtained for the maser data. The coordinates of I18286 adopted in the data correlation were the same as those for the VLBA data. The following coordinates of J1832 were adopted in the data correlation: $\alpha_{J2000} = 18^h32^m20^s.836564$, $\delta_{J2000} = -10^\circ35'11''.19990$.

In the EVN data reduction, in addition to the standard calibration procedure as described in Section 2.1, calibration of residual delays due to the ionosphere was also applied using the AIPS task TECOR (e.g., Vlemmings & van Langevelde 2007). Fringe fitting and self-calibration were carried out using

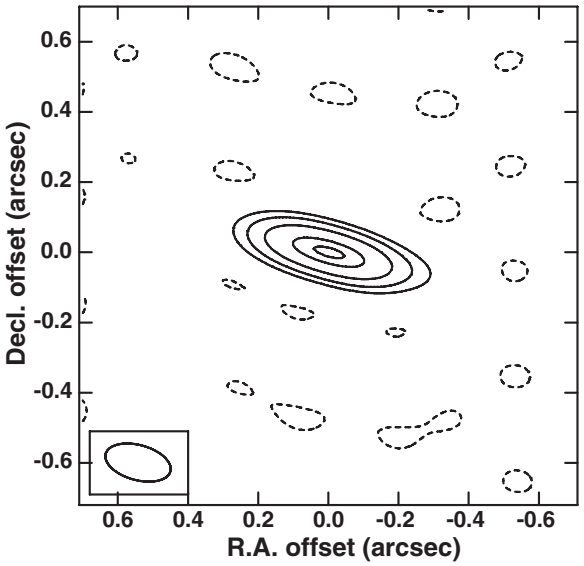

Figure 2. Contour map of J183220.8−103511 obtained in the EVN observation at 1.61 GHz. The contour levels are −0.5, 20, 40, 80 160, and 200 mJy beam^{-1}.

the data of J1832. For phase referencing, fringe fitting and self-calibration were made using the data of J1832. The obtained solutions for calibration were applied to the data of I18286. The image cube of the OH maser line was obtained in visibility deconvolution through the CLEAN algorithm. The uniformly weighted visibilities yielded a synthesized beam of 191 mas × 100 mas at a P.A. = 75° for the image of J1832, while the naturally weighted visibilities yielded a synthesized beam of 140 mas × 100 mas at a P.A. = −87° for the OH image cube of I18286. Figure 2 shows the contour map of J1832, which seems to be spatially resolved but exhibits a simple structure within the synthesized beam.

3. RESULTS AND DISCUSSION

3.1. Relative Proper Motions of H_2O Masers in IRAS 18286−0959

Many ($\gtrsim$90) H_2O maser features have been detected in the whole velocity range (-60 km s^{-1} $\leqslant$ $V_{\rm LSR}$ $\leqslant$ 160 km s^{-1}) in I18286 since its discovery (Deguchi et al. 2007; Papers I and II). Among the maser features detected in the three epochs in 2006–2007, we found the maser feature IRAS 18286−0959:I2013B-*46*, which was relatively isolated from other condensed groups of maser features and whose motion was unambiguously traced throughout all the three epochs. We chose this feature as a position reference to superpose the three maser maps and to measure relative proper motions of the maser features with respect to this reference feature. Hereafter, we always place this feature at the origin of the maser maps. Table 3 gives the parameters of H_2O maser features for which the proper motions were measured in these epochs.

Figure 3 shows the distribution of all maser features detected at any of the three epochs. Figure 4 shows the three-dimensional velocity field (LSR velocities and relative proper motions) of the H_2O masers whose proper motions were found in 2006–2007. The main characteristics of the maser distribution have persisted in the present observations and those in Papers I and II and were fitted to "double-helix" patterns in Paper I. We also calculated the projected jet patterns of the double-helix model in order to separate the outlier H_2O masers from the ones associated with

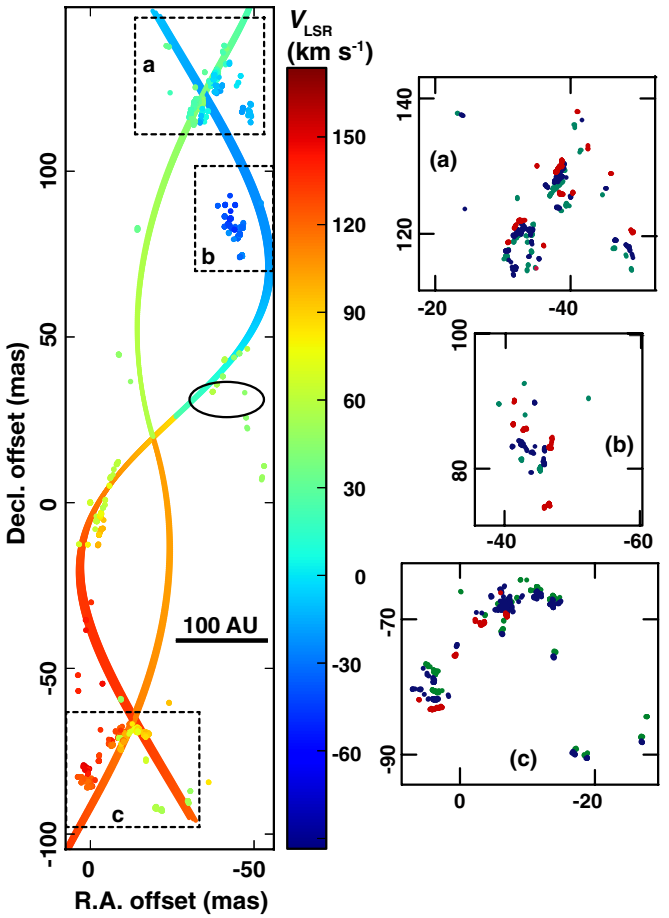

Figure 3. Locations of all H_2O maser spots detected in IRAS 18286−0959 at one of the observation epochs. The three-epoch maps are superposed using the common position-reference maser feature in the maser feature IRAS 18286−0959:I2013B-*46* located at the map origin. The maser spots are color coded as shown in a color bar and displayed in different symbols for the different epochs (but too small to be distinguished). The double-helix pattern shows the twin-jets model proposed by Paper I with parameters adjusted so as to fit the H_2O masers in the present data. The modeled patterns are modulated accounting for the maser proper motions. The location and the size of a black ellipse indicate the position of the OH maser spot at $V_{\rm LSR}$ = 39.5 km s^{-1} and its uncertainty, respectively. The right-side sub-panels (a), (b), (c) show the locations of H_2O maser spots in the dashed-square areas a, b, and c in the left panel, respectively, on 2006 September 15 (green circle), on 2006 November 9 (blue circle), and on 2007 February 3 (red circle).

the jets. Here, we adopted the jet model parameters slightly different from those of Paper I so as to better fit the jet patterns to the observed distribution of the H_2O masers. A sub-panel on the left in Figure 3 shows the distribution of the H_2O masers and the projected jet patterns of the double-helix model.

Note that the observed patterns of H_2O maser distribution were well fitted to the double-helix jets, although we shifted the systemic LSR velocities of the jets in the present model by $\sim$10 km s^{-1} from those of Paper I. The H_2O maser features exhibit several fragments of arc-shaped structures. As shown in sub-panels on the right in Figure 3, the maser motions are parallel to or have relatively small angular offsets from the elongation directions of these arc-shaped structures. This is considerably different from H_2O masers in star-forming regions, which show proper motions perpendicular to the directions of maser feature alignments (e.g., Imai et al. 2002). Because a precessing jet continuously changes the directions of ballistic motions of maser features one after another, the alignment of

Table 3
Relative Proper Motions of H_2O Maser Features Found in 2006–2007

Maser Feature No.[a]	Position Offset[b] (mas)		Relative Proper Motion[c] (mas yr^{-1})				Radial Motion[d] (km s^{-1})		Peak Intensity (Jy beam^{-1})		
(IRAS 18286−0959: I2013B-)	R.A.	Decl.	μ_X	$\sigma\mu_X$	μ_Y	$\sigma\mu_Y$	V_Z	ΔV_Z	Epoch 1	Epoch 2	Epoch 3
1	−42.34	83.53	−0.94	0.81	8.47	1.14	−45.77	3.27	···	0.02	0.14
2	−42.13	84.09	−3.50	0.81	7.35	0.62	−45.30	1.90	···	0.02	0.05
3	−42.32	83.61	−2.07	0.70	9.43	1.31	−42.98	3.05	···	0.01	0.09
4	−40.96	83.24	−0.31	0.37	13.71	0.54	−39.29	2.63	···	0.04	0.08
5	−44.96	79.98	−4.02	0.22	7.37	0.65	−35.70	5.90	1.26	1.03	0.04
6	−45.71	82.67	−4.28	0.37	7.36	1.19	−31.66	2.53	···	0.06	0.03
7	−45.02	79.73	−4.02	0.14	8.08	0.29	−30.44	2.46	0.20	0.03	0.07
8	−46.24	117.92	−2.80	0.52	7.73	0.39	−20.37	4.11	0.13	0.13	···
9	−48.22	118.41	−3.14	0.56	7.31	0.84	−13.19	1.89	···	0.10	0.31
10	−48.87	114.91	−1.29	0.92	12.98	2.13	−12.54	1.16	0.11	0.04	···
11	−48.11	116.95	−2.67	0.23	8.26	0.40	−10.59	1.33	0.13	0.03	0.10
12	−33.66	115.49	−1.39	0.81	8.39	1.37	−10.54	0.95	0.13	0.02	···
13	−39.25	124.38	−2.47	0.19	3.45	0.31	−10.06	2.03	0.18	0.03	0.26
14	−37.90	123.96	−1.87	0.91	7.59	0.43	−9.96	2.63	···	0.10	0.19
15	−37.36	126.71	−1.46	0.22	5.99	0.21	−3.92	4.55	0.59	0.18	1.36
16	−44.66	125.81	−2.95	0.18	8.48	0.18	0.66	0.77	0.03	0.08	0.22
17	−37.61	127.74	−1.88	0.25	7.47	0.45	3.24	2.32	···	0.09	0.13
18	−34.16	117.41	−0.31	0.46	8.81	0.91	4.24	2.32	0.17	0.02	···
19	−37.34	126.71	−1.40	0.26	7.15	0.36	6.56	2.14	0.03	0.14	0.06
20	−34.70	115.01	−2.92	0.24	7.69	0.37	8.04	0.98	0.05	0.03	0.04
21	−37.55	126.69	−2.62	0.52	8.89	0.71	11.84	2.53	2.99	0.10	···
22	−37.75	126.84	−1.46	0.26	7.54	0.34	14.91	6.32	0.87	0.15	0.97
23	−38.22	127.23	−1.31	1.52	6.23	0.99	17.09	1.79	0.09	0.30	···
24	−36.99	125.89	1.98	1.08	7.17	0.53	17.31	2.11	0.82	0.15	···
25	−38.42	127.48	0.08	0.37	5.58	0.44	17.36	3.23	0.17	0.46	0.16
26	−30.34	116.71	−0.67	0.81	5.23	1.30	21.67	1.69	0.08	0.17	···
27	−30.57	116.57	−0.19	0.23	4.98	0.17	23.04	1.62	0.05	0.07	0.23
28	−37.90	127.29	−1.88	0.16	9.23	0.19	24.82	6.53	0.13	0.16	1.20
29	−40.51	136.21	−0.90	0.36	4.44	0.56	26.36	0.73	0.03	···	0.13
30	−31.51	118.89	−0.57	0.27	5.36	0.43	26.81	2.25	0.08	0.11	0.18
31	−32.09	120.65	−1.27	0.37	4.95	1.08	28.69	3.47	···	0.57	0.36
32	−32.14	119.78	−0.70	0.31	4.84	0.28	32.05	4.49	0.75	0.46	0.79
33	−23.21	137.87	−4.73	0.58	−1.77	0.60	35.41	0.94	0.08	0.06	···
34	−33.24	120.90	0.65	1.29	4.19	0.73	36.93	1.37	···	0.05	0.35
35	−30.56	116.50	−3.78	1.61	−4.37	2.34	37.24	0.73	0.05	0.01	···
36	−38.95	129.56	−0.55	0.38	5.54	0.50	39.15	2.11	0.56	0.12	···
37	−34.31	119.93	−0.68	0.90	5.43	1.09	48.70	2.63	0.06	0.05	···
38	−33.58	118.80	−2.92	0.80	7.26	1.42	54.89	1.26	0.03	0.09	···
39	−29.92	−89.99	−0.85	0.73	−4.35	0.77	57.73	1.68	0.09	0.04	···
40	−21.76	−92.50	−1.07	0.66	−2.73	1.01	59.01	1.26	0.04	0.03	···
41	−20.00	−91.84	−0.56	0.87	−3.64	1.01	61.56	1.89	0.13	0.06	···
42	−7.13	9.99	2.45	0.26	−6.03	0.48	62.17	0.91	0.05	0.03	0.44
43	−8.51	12.31	1.53	1.06	−2.50	1.37	64.49	1.48	···	0.29	0.08
44	−8.86	−70.39	0.98	1.54	−4.19	0.32	68.28	2.43	0.11	0.13	···
45	−17.04	−77.46	0.20	1.08	−3.66	1.24	70.18	0.42	0.04	0.02	···
46	0.00	0.00	0.00	0.13	0.00	0.18	70.81	1.40	0.47	0.37	0.54
47	−11.33	−69.49	−3.15	0.48	−2.14	0.78	73.72	0.63	0.09	0.02	···
48	−9.92	−70.40	1.72	1.04	−4.36	0.78	76.86	4.22	1.18	0.12	···
49	−9.01	−70.60	−5.98	1.22	−3.21	0.76	81.64	7.59	0.18	2.62	···
50	−14.35	−67.94	0.26	0.69	−7.44	1.90	83.44	2.32	0.43	0.06	···
51	−14.64	−68.63	3.66	1.28	−3.19	0.94	87.43	2.63	0.08	0.19	···
52	−3.29	−3.77	6.13	0.32	−8.04	0.56	89.90	2.42	···	0.29	0.22
53	−14.86	−68.21	3.20	2.55	−4.51	1.34	89.99	2.63	0.19	0.05	···
54	−16.70	−70.12	−0.93	1.46	−3.22	1.57	92.09	3.80	0.77	0.34	···
55	−3.23	−4.04	1.23	0.28	−0.42	0.75	92.61	2.53	···	0.27	0.62
56	−14.30	−68.02	−1.50	0.41	−1.62	1.14	93.33	2.53	0.23	0.32	···
57	−3.19	−4.11	1.46	0.20	−1.34	0.32	93.93	3.05	···	0.30	0.64
58	−17.10	−69.57	−4.11	2.12	−3.32	0.88	96.09	1.58	0.12	0.12	···
59	−3.72	−7.82	2.51	0.32	−2.86	0.63	100.51	1.37	···	0.05	0.08
60	−16.73	−69.10	−0.47	0.38	−3.09	0.41	101.24	2.00	0.50	0.04	···
61	−9.33	−74.07	−0.69	0.54	−3.40	0.45	101.89	1.47	0.10	0.09	···
62	−9.87	−70.89	−1.10	0.12	−3.29	0.11	108.45	6.10	1.51	0.29	0.76
63	−9.92	−70.96	−1.12	0.27	−4.52	0.70	118.16	6.01	···	0.07	0.86
64	−9.97	−70.15	−0.83	0.35	−4.21	0.39	121.32	6.46	0.37	0.13	0.24

Table 3
(Continued)

Maser Feature No.[a]	Position Offset[b] (mas)		Relative Proper Motion[c] (mas yr^{-1})				Radial Motion[d] (km s^{-1})		Peak Intensity (Jy beam^{-1})		
(IRAS 18286−0959: I2013B-)	R.A.	Decl.	μ_X	$\sigma\mu_X$	μ_Y	$\sigma\mu_Y$	V_Z	ΔV_Z	Epoch 1	Epoch 2	Epoch 3
65	0.93	−84.17	−1.23	1.12	−7.07	0.27	124.51	1.06	···	0.10	0.12
66	1.49	−84.16	−1.58	0.39	−7.62	0.54	125.35	0.73	···	0.02	0.15
67	0.77	−84.23	−0.27	1.20	−7.03	0.49	127.25	1.89	···	0.13	0.07
68	−8.70	−70.44	2.13	1.89	−4.21	1.61	130.18	2.21	0.08	0.02	···
69	0.92	−83.20	0.13	0.78	−7.19	0.25	130.21	1.97	0.20	0.11	0.10
70	0.88	−83.21	−2.87	0.65	−6.19	0.21	131.64	2.39	0.35	0.05	0.76
71	0.46	−83.46	−0.02	1.51	−5.21	0.80	134.17	1.90	0.09	0.03	···
72	−2.70	−76.32	0.84	0.45	−6.74	0.59	137.37	1.69	···	0.02	0.04
73	0.68	−80.70	0.54	0.20	−6.63	0.36	150.70	2.63	0.25	0.10	···
74	0.69	−80.65	0.81	0.84	−7.00	0.99	153.39	2.01	0.05	0.09	···
75	0.75	−80.38	−0.63	0.82	−7.23	1.13	155.52	3.80	0.06	0.09	···
76	1.42	−79.61	−3.79	0.94	−9.42	0.93	158.66	2.16	0.03	0.02	···
77	1.81	−79.29	−2.09	0.55	−9.81	1.35	159.71	0.42	0.04	0.01	···

Notes.
[a] Maser features detected in IRAS 18286−0959. The features are designated as IRAS 18286−0959:I2013-*N*, where *N* is the ordinal source number given in this column (I2013B stands for sources found by Imai et al. and listed in 2013 after another maser identification by Paper II.
[b] Relative value with respect to the location of the position-reference maser feature: IRAS 18286−0959:I2013B-*46*.
[c] Relative value with respect to the motion of the position-reference maser feature: IRAS 18286−0959:I2013B-*46*.
[d] Local-standard-of-rest velocity.

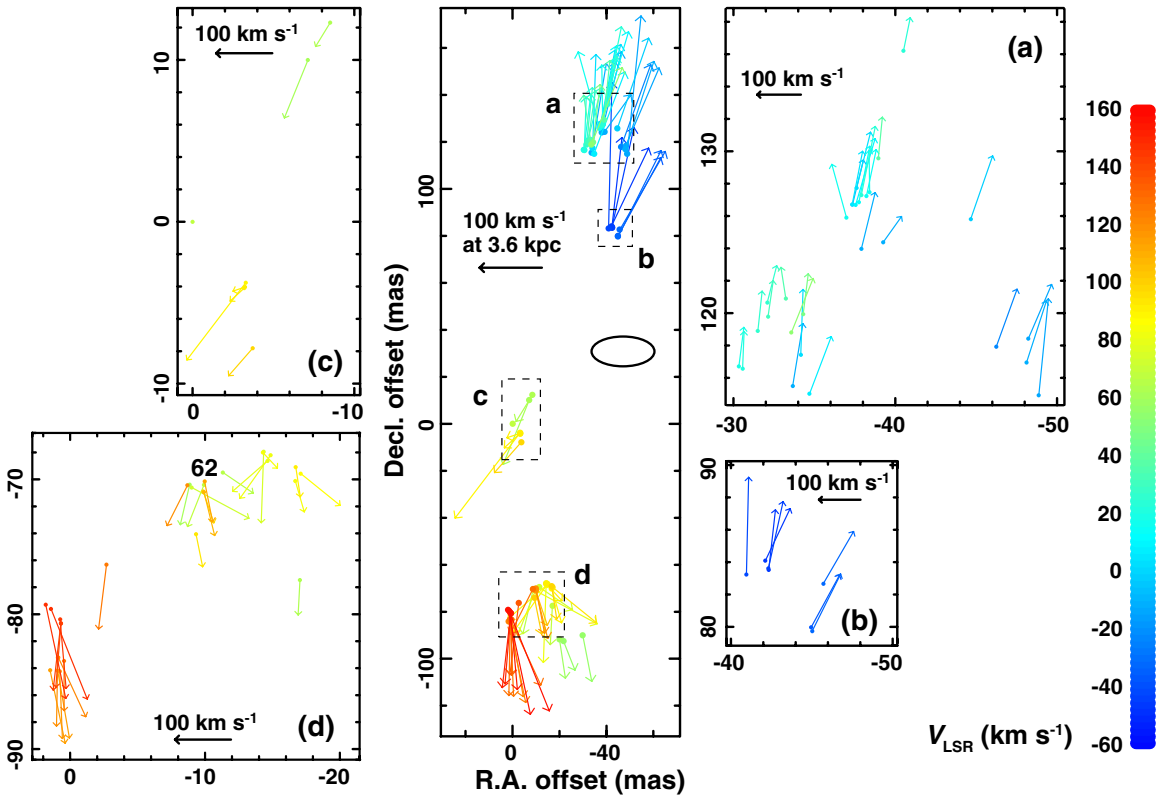

Figure 4. Relative proper motions of H_2O masers in IRAS 18286−0959. The position, the length, and the direction of an arrow indicates the position of the maser feature at its first detection epoch, the speed, and the direction of the proper-motion vector, respectively. A transverse velocity of 100 km s^{-1}, corresponding to a proper motion of 5.86 mas yr^{-1}, is displayed with a black arrow. For clarity, four regions of maser feature clusters are zoomed up in the sub-panels (a)–(d). The maser feature IRAS 18286−0959:I2013B-*62*, which explicitly appears in the main text, is labeled by "62" in the sub-panel (d). A black ellipse is as the same as that in Figure 3.

maser features has an angular offset from the maser motions, which is proportional to the projected angular velocity of the jet's precession. The maser excitation may occur somehow randomly at different distances from the originating point of the jet and such a situation may prevent from the exact alignment of the maser features on the modeled jet patterns. However, the observed microscopic patterns of masers are roughly found along the double-helix patterns, consistent with the suggestion that the precessing twin jets were formed and they formed the observed microscopic patterns.

It is noteworthy that all of the maser features with proper motions measured in Paper I are associated with the double-helix jets, except the position-reference maser feature. Paper I investigated the maser features which were detectable at three or

Table 4
Relative Proper Motions of the Short-lived H_2O Maser Features Found in 2008–2009

Maser Feature No.[a]	Position Offset[b] (mas)		Relative Proper Motion[c] (mas yr^{-1})				Radial Motion[d] (km s^{-1})		Peak Intensity at 6 Epochs (Jy beam^{-1})					
(IRAS 18286−0959: I2013B-)	R.A.	Decl.	μ_X	$\sigma\mu_X$	μ_Y	$\sigma\mu_Y$	V_Z	ΔV_Z	EP1	EP2	EP3	EP4	EP5	EP6
78	−0.34	−0.87	−0.09	0.28	−0.18	0.25	48.84	−0.36	···	0.63	0.38	···	···	···
79	−0.38	−0.73	0.00	0.03	−0.06	0.20	49.25	−0.38	···	···	···	0.46	···	0.35
80	0.00	0.00	0.00	0.43	0.00	0.21	51.57	0.00	4.35	3.72	1.13	0.54	4.24	1.00
81	6.40	−44.62	0.98	0.44	−1.59	0.39	62.54	6.48	···	···	0.91	2.13	···	···
82	1.20	−33.72	0.48	0.59	1.25	0.56	64.67	1.23	5.10	4.09	···	···	···	···
83	5.33	−39.77	0.53	0.15	0.02	0.15	68.03	5.45	···	···	···	0.16	···	1.78
84	13.40	−59.95	−0.87	0.35	−0.10	0.62	70.79	13.35	0.39	0.40	···	···	···	···
85	5.20	−40.97	1.59	0.08	−1.80	0.15	71.21	5.78	0.96	0.52	0.52	0.35	···	···
86	11.25	−13.58	0.14	0.10	0.76	0.08	75.43	11.31	0.32	···	0.34	0.60	···	···
87	13.68	−63.64	0.38	0.17	0.26	0.17	79.85	13.77	···	···	···	0.63	···	1.23
88	8.28	−53.49	2.02	0.83	−1.06	0.78	89.35	8.39	3.66	10.94	···	···	···	···
89	8.85	−60.20	1.45	1.09	−0.10	0.91	92.73	8.93	8.24	4.17	···	···	···	···
90	10.32	−59.70	−1.04	0.31	−1.31	0.46	96.11	10.18	···	···	···	···	3.83	0.93
91	9.74	−58.56	1.93	0.34	−2.31	0.19	98.43	9.99	···	···	···	···	1.82	1.59
92	7.14	−55.33	−0.96	0.91	−1.54	0.86	107.08	7.09	0.46	0.64	···	···	···	···

Notes.
[a] Maser features detected in IRAS 18286−0959. The features are designated as IRAS 18286−0959:I2013-*N*, where *N* is the ordinal source number given in this column (I2013B stands for sources found by Imai et al. and listed in 2013 after another maser identification by Paper II).
[b] Relative value with respect to the location of the position-reference maser feature: IRAS 18286−0959:I2013B-*80*.
[c] Relative value with respect to the motion of the position-reference maser feature: IRAS 18286−0959:I2013B-*80*.
[d] Local-standard-of-rest velocity.

more epochs. In the present work, the maser features survived at only two epochs were accepted as data of proper-motion measurement as long as each of them is stable within 0.5 mas in position and 0.5 km s^{-1} in velocity between two consecutive epochs. Before the new identification of maser proper motions was attempted, we flagged the maser features that have already been used in Paper I. These criteria of identification of maser proper motions and the flagging procedure inevitably pick up the "outlier" H_2O maser features with slow proper motions (see Sections 1 and 3.3). Table 4 gives the list of the newly identified maser proper motions. Except the maser features: IRAS 18286−0959:I2013B-*80*, *85*, and *86*, which were detected at three epochs or more, the maser features with the proper motions were detected at only two epochs as mentioned above, indicating their short lifetimes ($t \lesssim 3$ months).

The maser proper-motion distribution shown in Figure 4 is roughly consistent with those in Papers I and II. If we can find the same maser feature (or the same proper-motion data point) in these data, these distributions can be displayed on a common coordinate system. However, because the observation seasons of these data were significantly separated (season separations of 0.8 yr or longer), it is unclear whether the maser features for position referencing really survived in the entire period. Nevertheless, carefully checking persistent distribution of the maser features in these seasons and equality of LSR velocities and relative intensities of the masers, we selected the feature at $V_{\rm LSR} = 108.5$ km s^{-1} and the position (−9.9, −70.9) mas in 2006–2007 (IRAS 18286−0959:I2013B-*62* in this paper) and that at $V_{\rm LSR} = 108.1$ km s^{-1} at the position (−1.7, −124.5) mas in 2008–2009 (Paper I), and assumed that they are at least associated with a common maser region (condensed feature cluster). Taking into account its relative proper motion with respect to the position-reference feature, (−1.1, −3.3) mas yr^{-1}as well, we estimated the shift from the coordinate system in 2008–2009 to that in 2006–2007 to be about (9, −55) mas. Similarly, we selected the maser feature at $V_{\rm LSR} = 70.8$ km s^{-1}, at the map origin (IRAS 18286−0959:I2013B-*46* in this paper) and that at $V_{\rm LSR} = 71.0$ km s^{-1}, (54.8, −11.8) mas in 2007–2008 (Paper II) and adopted the same assumption for the map superposition as mentioned above.

Note that if two H_2O maser features observed in different seasons are really the same one, the measured proper-motion vector in one season can be converted to that measured in another season by subtracting the difference of the measured vectors. However, if the difference of the two proper-motion vectors is large among the three observations, it is difficult to judge that these masers are associated with the same maser feature and to adopt such a proper-motion conversion. The difference of the proper-motion vectors between IRAS 18286−0959:I2013B-*62* in this paper and the $V_{\rm LSR} = 108.1$ km s^{-1} component at the position (−1.7, −124.5) mas in Paper I is $(\Delta\mu_X, \Delta\mu_Y) = (0.90, 2.55)$ mas yr^{-1}, or $(\Delta V_X, \Delta V_Y) = (15, 44)$ km s^{-1}at 3.6 kpc. Because the position-reference features, on the other hand, may have much smaller intrinsic motions in the maser cluster, the former masers are likely different ones. In this paper, we assume that the intrinsic proper motions of the position-reference features in Papers I, II, and this paper are nearly zero. Then we directly compare the proper motions of other masers among these papers (Section 3.3). The zero motion approximation is supported, without any coordinate conversion, by the point-symmetric motions of maser features in the jets with respect to the central region where the OH maser emission is located as shown soon later.

3.2. The Location of the OH Maser Emission in IRAS 18286−0959

Only one OH maser feature was clearly detected in the spectrum at $V_{\rm LSR} = 39.5$ km s^{-1}, which is consistent with that found in a previous observation (Sevenster et al. 2001). Figure 5 shows the contour map of the 39.5 km s^{-1} maser component and the spectrum synthesized at the maser location. This component

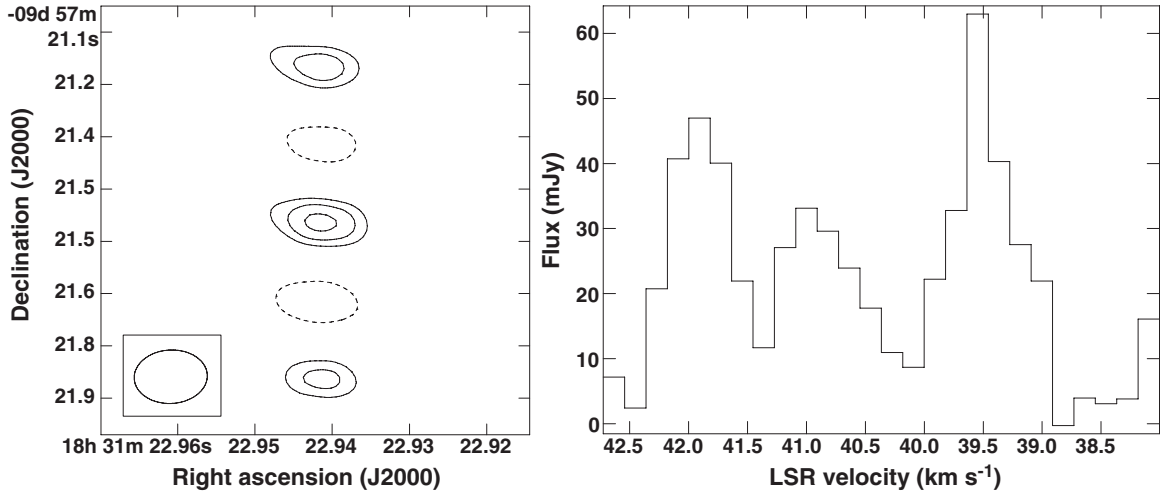

Figure 5. 1612 MHz OH masers in IRAS 18286−0959 detected with the EVN. Left: contour map of the maser emission at $V_{\rm LSR} = 39.5$ km s^{-1}. The contour levels are −55, 55, 70, and 85 mJy beam^{-1}. The bottom left box shows the synthesized beam pattern of the map. Right: spectrum of the maser emission synthesized on the region of the 39.5 km s^{-1} component.

was detected in the phase-referenced image at 93 mJy beam^{-1} with a signal-to-noise ratio of 7.5. We also marginally detected the emission at $V_{\rm LSR} = 41.9$ km s^{-1}, whose location is consistent with that of the 39.5 km s^{-1} component.

By the astrometric observation, the absolute coordinates of the 39.5 km s^{-1} component in 2007 June were determined to be $\alpha_{\rm J2000} = 18^{\rm h}31^{\rm m}22\overset{\rm s}{.}94145 \pm 0\overset{\rm s}{.}00083$, $\delta_{\rm J2000} = -09^\circ57'21\overset{''}{.}4642 \pm 0\overset{''}{.}0056$.

On the other hand, it is impossible to precisely determine the absolute coordinates of the I18286 H_2O masers in the present VLBA observations alone without the phase-referencing technique in the data analysis. Instead, we cited the coordinates and absolute proper motion of one of the maser features detected in the VLBI Exploration of Radio Astrometry observation on 2007 October 23 (Paper II). The mean absolute coordinates of the maser feature containing the $V_{\rm LSR} = 53.0$–53.4 km s^{-1} components in Paper II (IRAS 18286−0959:I2013-*14*) were (on 2007 June 10 if it appeared) $\alpha_{\rm J2000} = 18^{\rm h}31^{\rm m}22\overset{\rm s}{.}938027 \pm 0\overset{\rm s}{.}000009$, $\delta_{\rm J2000} = -09^\circ57'21\overset{''}{.}46988 \pm 0\overset{''}{.}00011$. Taking into account the persistent distribution of the maser features for at least a half-year, some features detected in Paper II likely correspond to those detected in the present observations. Thus we find that the position-reference maser feature in this paper, IRAS 18286−0959:I2013B-*46*, likely corresponds to the maser feature IRAS 18286−0959:I2013-*19* in Paper II. The absolute coordinates of the former feature are estimated to be (on 2007 June 10) $\alpha_{\rm J2000} = 18^{\rm h}31^{\rm m}22\overset{\rm s}{.}94103 \pm 0\overset{\rm s}{.}00006$, $\delta_{\rm J2000} = -09^\circ57'21\overset{''}{.}4815 \pm 0\overset{''}{.}0004$. The uncertainty of the H_2O maser coordinates is mainly attributed to the uncertainty of the intrinsic absolute proper motion of this feature. The uncertainty of the absolute OH maser coordinates is thus mainly dominated by the signal-to-noise ratio of the detection, $(\sigma_x, \sigma_y) \simeq (12, 4)$ mas. It is still small enough to compare the coordinates between the H_2O and OH masers. Combining the information of these absolute coordinates of the H_2O and OH masers and comparing the H_2O maser distribution found in Paper I with that in this paper, the location of the OH maser emission was determined on the coordinate systems of the maps of H_2O masers found in 2006–2007 and 2008–2009.

The location of the OH maser emission is closer to the originating point of the younger jet (right side: jet 1) of the double-helix model of Paper I. If the central star is moving westward, as suggested by Paper I, the estimated present position of the star is well consistent with the position of the OH maser. If OH masers are excited by infrared radiation of the star and they are radially beamed (e.g., Elitzur 1992), they well pinpoint the location of the star. Although the blueshifted and redshifted components of OH masers often have more or less a certain angular offset, this is much smaller than the separation of the double lobes as seen in the water fountain jet (e.g., Imai et al. 2002, 2013a). Paper I estimated the systemic LSR velocities of the two jets, $V_{\rm LSR}$(jet 1) $\approx$ 47 km s^{-1} and $V_{\rm LSR}$(jet 2) $\approx$ 54–61 km s^{-1}. The modeled two jets in this paper suggest more redshifted systemic velocities. In any case, these suggest that the OH maser in I18286 should be a blueshifted component and the expansion velocity of the OH envelope is estimated to be $V_{\rm exp} \approx$ 10–30 km s^{-1}, close to a typical value of CSE expansion velocities of OH/IR stars. We note that Imai et al. (2009) detected a CO emission line toward I18286 at $V_{\rm LSR} \approx$ 65 km s^{-1}. However, it may originate from foreground and/or background interstellar molecular clouds, which were spatially resolved out by a synthesized beam of the Combined Array for Research in Millimeter-wave Astronomy (J. Nakashima 2012, private communication).

3.3. Outlier H_2O Maser Features in IRAS 18286−0959

We suppose that some of the "outlier" H_2O maser features in I18286 are associated with the OH envelope. They have LSR velocities nearly equal to the systemic velocity and small three-dimensional velocities, and they are located in or around the OH envelope. The H_2O maser feature used for the trigonometric parallax measurement in Paper II (IRAS 18286−0959: I2013-*14*; and a few more features) and that used as a position reference in Paper I had LSR velocities of $V_{\rm LSR} \simeq$ 53 and 52 km s^{-1}, respectively. They also had small differences of three-dimensional motion vectors from the systemic three-dimensional motion of the jet driving source (Paper II), suggesting $V_{\rm exp} \lesssim$ 30 km s^{-1}. These facts meet the criteria of the outliers. One of the H_2O masers in W 43A and some groups of the masers in IRAS 18460−0161 also met the criteria (Imai 2007; Imai et al. 2013a). However,

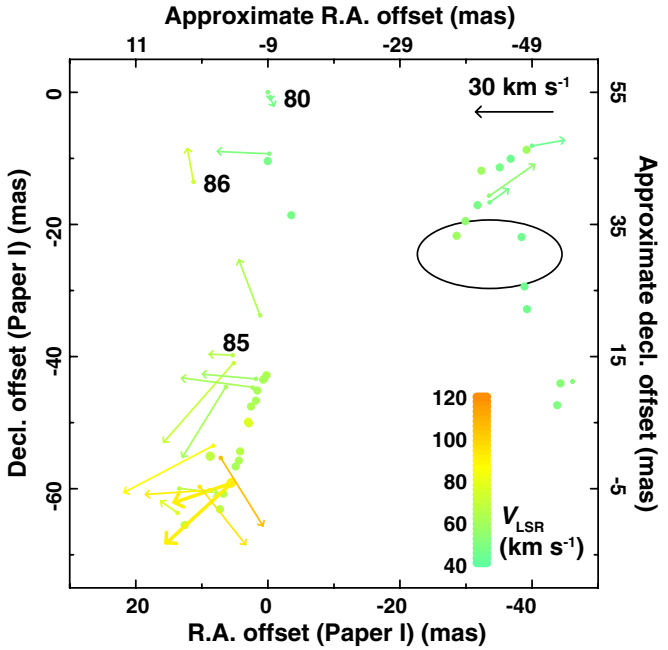

Figure 6. Same as Figure 4 but for the short-lived H_2O masers identified in Paper I and the low-velocity H_2O masers identified in Paper II. The coordinates systems of the maser maps in Papers I and II are approximately converted to that adopted in the present paper (see the main text). The labels of the original coordinate offsets are shown only for the system of Paper I. Filled circles and thicker arrows denote as the same *outlier* masers as the outlier H_2O masers displayed in Figure 4(c). A number label is the same as that assigned to the maser feature listed in Table 3. The three features with the number labels in this figure explicitly appear in the main text. A black ellipse is as the same as those in Figures 3 and 4.

these maser features seem to have relatively short lifetimes and more intensive monitoring VLBI observations are necessary to measure proper motions of such features. Such a case is also seen in the present data in 2006–2007, in which we could find only three proper motions of maser features identified as such outliers. Nevertheless, with the data of Paper I (2008–2009), we find that a group of the short-lived maser features ($t \lesssim 3$ months), except two maser features that are associated with the jets and not listed in Table 4, are located close to the center of the originating points of the jets and to the OH maser emission. This has a clear contrast to the situation found in Paper I, in which all of the long-lived maser features ($t \gtrsim 5$ months; except the position-reference maser feature) were associated with the modeled jets. We also find a group of low-velocity masers in the map of Paper II.

Figure 6 shows the map of the short-lived H_2O masers found in Paper I, the low-velocity masers found in Paper II, and their proper motions (if available). The maser features in the eastern side are located very close to one of the jet major axes. However, some of such maser features, as well as those within 20 mas of the location of the OH maser emission, have LSR velocities within 30 km s^{-1} of the systemic velocity of the jet. The proper motions of these maser features are equal to or slower than 30 km s^{-1}, much lower than those of features associated with the jet ($V > 100$ km s^{-1}). They also marginally exhibit expanding motions so as to be driven by the star near the OH maser source. It is difficult to construct an expanding flow model as made in previous papers (the latest example is shown in Imai et al. 2013a) because the number of these H_2O masers is insufficient (<20) and, more importantly, the uncertainty of the relative proper motions may be very large among the masers cited from the different data.

Figure 7 shows the position–velocity and proper-motion–velocity diagrams of H_2O masers in I18286. In this figure, we attempted to identify such outliers, including the maser features whose proper motions could not be measured. A group of maser features with $-50\,\mathrm{mas} \lesssim X$ (R.A. offset) $\lesssim 50$ mas, $-50\,\mathrm{mas} \lesssim Y$ (decl. offset) $\lesssim 50$ mas, $-4\,\mathrm{mas\,yr^{-1}} \lesssim \mu_x$ (proper motion in the right ascension direction) $\lesssim 4$ mas yr^{-1}, $-4\,\mathrm{mas\,yr^{-1}} \lesssim \mu_y$ (proper motion in the declination direction) $\lesssim 4$ mas yr^{-1}, and $30\,\mathrm{km\,s^{-1}} \lesssim V_{\mathrm{LSR}} \lesssim 80$ km s^{-1}, can be members of the outliers and are denoted by black (with a measured proper motion) and gray (without one) cross symbols in Figure 7. They are marginally distinguishable from other maser features especially in the (X, μ_y), (Y, μ_y), (X, V_z), and (Y, V_z) plots. The apparent extension of the outlier candidates in I18286 is about 60 mas, corresponding to a linear scale of about 220 AU. Note that the expansion velocity estimated from these H_2O masers ($V_{\mathrm{exp}} \lesssim 30\,\mathrm{km\,s^{-1}}$) is comparable to or higher than that of the OH envelope ($V_{\mathrm{exp}} \lesssim 20\,\mathrm{km\,s^{-1}}$). These properties are consistent with those found in other water fountains: W 43A and IRAS 18460−0151 (Imai 2007; Imai et al. 2013a). Because the spatiokinematical structure of the outlier H_2O masers resemble those in OH/IR stars, it is suggested that the relic AGB CSE in I18286 is still in a young stage before such outlier H_2O masers disappear. Taking into account the possible duration timescale of a relic CSE wind as found in OH/IR stars ($\lesssim$1000 yr e.g., Lewis 2001), such relic CSEs should be persistent in the water fountain phase (likely $\lesssim$100 yr) with a high possibility.

However, the evidence of the existence of a relic CSE as shown is not clearly revealed in Figure 7 although a group of low-velocity outlier H_2O masers are found in the vicinity of the originating points of the high-velocity jets as shown in Figure 6. The data points in Figure 7 have too large scatter, making it difficult to distinguish the outliers from the masers associated with the jets. The outlier masers with the measured proper motions are located on one of the two jets (region c in Figure 4) and some of them have proper-motion vectors parallel to the jet axis. In the case of IRAS 16342−3814 (Claussen et al. 2009), the OH expansion velocity achieves $V_{\mathrm{exp}} \approx 70$ km s^{-1}, comparable to the jet velocity. If this is the case of I18286, the outlier masers may be suggested to be associated with an equatorial flow, a by-product of the newly formed collimated jet. However, it is difficult to further differentiate the H_2O masers associated with the equatorial flow from those with the highly collimated jet unless a sufficient number of the former H_2O masers are detected and their proper motions are measured. Because the majority of such H_2O maser features are short-lived (Section 3.1), more intensive (biweekly to monthly) VLBI observations are necessary to trace a larger number of such maser proper motions.

Thus it is interesting to know when a relic CSE is displaced by an equatorial flow. In fact, H_2O masers associated with PNe or PN candidates exhibit a variety of velocity coverages, from a narrow case ($V_{\mathrm{exp}} < 10$ km s^{-1}) to a wide one ($V_{\mathrm{exp}} > 40$ km s^{-1}; e.g., Miranda et al. 2001; Suárez et al. 2009, 2012; Tafoya et al. 2011). Interestingly, these H_2O masers (including high-velocity components) are not necessarily associated with bipolar lobes of optical, infrared, and/or radio emission while H_2O masers in the water fountains have a tight correlation with the jets except the outlier H_2O masers described in this paper. Therefore, it is important to determine whether such high-velocity H_2O masers in PNe (or PN candidates) are

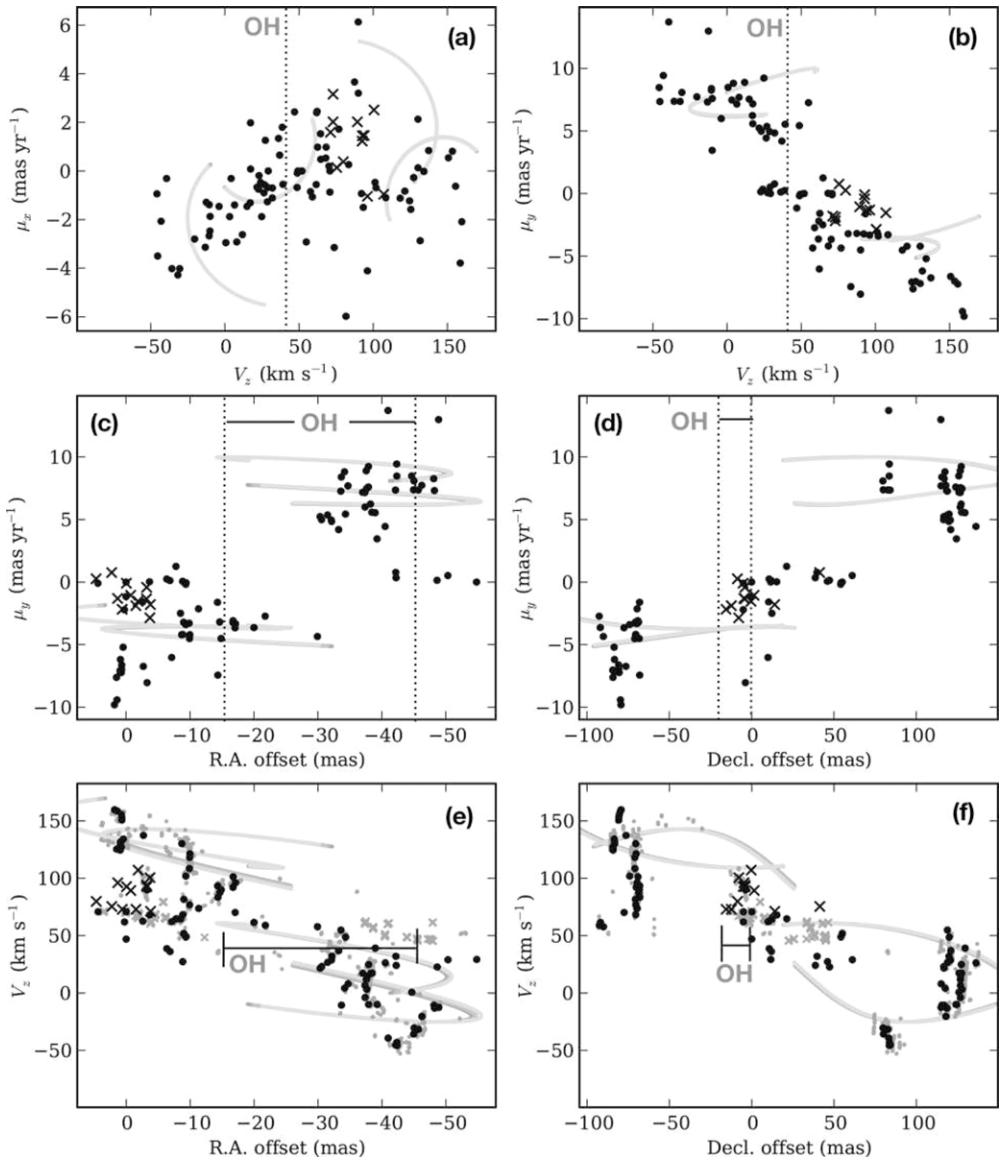

Figure 7. Diagrams of combinations among maser feature positions and motions. All H_2O maser features, with measured proper motions (black symbols) and without ones (gray symbols), are plotted. The data points of the short-lived, low-velocity maser features obtained from the data of Paper I and those of the low-velocity maser features found in Paper II, which are displayed in Figure 6, are also added. They are also denoted by black cross symbols. The LSR velocity of the OH maser line ($V_{\rm LSR} = 39.5$ km s^{-1}) is indicated by a dotted line. The position of the OH maser emission with respect to the H_2O maser features is indicated by a bar, whose length indicates the position uncertainty. The maser distribution patterns expected from the precessing double-jet model are displayed in curved thick lines. The "outlier" masers are displayed in cross symbols while others in filled circles.

associated with a highly collimated jet, or with an equatorial flow.

4. CONCLUSIONS

In the present EVN observation, we pinpointed the location of the 1612 MHz OH maser source in the three-dimensional velocity field traced by the H_2O masers. The existence of the OH maser emission itself indicates the presence of a relic AGB wind from this object. Using the VLBA data of H_2O masers at nine epochs, we newly identified a group of short-lived H_2O maser features, which were located in the vicinity of the central region of the H_2O maser distribution and close to the OH maser source. Many of the short-lived H_2O masers had three-dimensional velocities ($\lesssim$30 km s^{-1}) much lower than those of the masers associated with the high-velocity jets (>100 km s^{-1}). Together with the maser features whose LSR velocities are close to the systemic velocity ($30 \lesssim V_{\rm LSR} \lesssim 80$ km s^{-1}) but which do not have their proper-motion data, such "outlier" H_2O masers are likely associated with the relic AGB CSE. This suggests that I18286 harbors a relic AGB CSE similar to the cases of W 43A and IRAS 18460−0151. This fact indicates that a spherical slow outflow as seen in OH/IR stars are deformed to a relic envelope by precessing, collimated jets.

The VLBA/National Radio Astronomy Observatory is a facility of the National Science Foundation, operated under a cooperative agreement by Associated Universities, Inc. The European VLBI Network (EVN) is a joint facility of European, Chinese, South African and other radio astronomy institutes funded by their national research councils. H.I. has been supported financially by Grant-in-Aid for Young Scientists (B) from the Ministry of Education, Culture, Sports, Science, and

Technology (18740109) and for stay at ICRAR by the Strategic Young Researcher Overseas Visits Program for Accelerating Brain Circulation funded by Japan Society for the Promotion of Science (JSPS). H.I. and S.D. have been financially supported by Grant-in-Aid for Scientific Research from JSPS (20540234). B.Y. acknowledges the support by the HKU SPACE Research Fund. J.N. has been supported by the Research Grants Council of Hong Kong (project code: HKU 703308P, HKU 704209P, HKU 704710P, and HKU 704411P), and the Small Project Funding of The University of Hong Kong (201007176004).

REFERENCES

Amiri, N., Vlemmings, W. H. T., & van Langevelde, H. J. 2010, A&A, 509, A26
Amiri, N., Vlemmings, W. H. T., & van Langevelde, H. J. 2011, A&A, 532, A149
Beasley, A. J., & Conway, J. E. 1995, in ASP Conf. Ser. 82, Very Long Baseline Interferometry and the VLBA, ed. J. A. Zensus, P. J. Diamond, & P. J. Napier (San Francisco, CA: ASP), 327
Boboltz, D. A., & Marvel, K. B. 2005, ApJL, 627, L45
Claussen, M., Sahai, R., & Morris, M. R. 2009, ApJ, 691, 219
Day, F. M., Pihlström, Y. M., Claussen, M. J., & Sahai, R. 2010, ApJ, 713, 986
Deguchi, S., Nakashima, J., Kwok, S., & Koning, N. 2007, ApJ, 664, 1130
de Gregorio-Monsalvo, I., Gómez, Y., Angalada, G., et al. 2004, ApJ, 601, 921
Desmurs, J.-F. 2012, in Proc. IAU Symp. 287, Cosmic Masers—from OH to H_0, ed. R. S. Booth, E. M. L. Humphreys, & W. H. T. Vlemmings (Cambridge: Cambridge Univ. Press), 217
Elitzur, M. 1992, Astronomical Masers (Dordrecht: Kluwer)
Huggins, P. J. 2007, ApJ, 663, 342
Imai, H. 2007, in IAU Symp. 242, Astrophysical Masers and their Environments, ed. W. Baan & J. Chapman (Cambridge: Cambridge Univ. Press), 279
Imai, H., Deguchi, S., Nakashima, J., Kwok, S., & Diamond, P. J. 2013a, ApJ, submitted
Imai, H., Deguchi, S., & Sasao, T. 2002, ApJ, 567, 971
Imai, H., Diamond, P. J., Nakashima, J., Kwok, S., & Deguchi, S. 2008, in Proc. 9th European VLBI Network Symposium on the Role of VLBI in the Golden Age for Radio Astronomy and EVN Users Meeting, PoS(IX EVN Symposium) (Trieste, Italy: SISSA), 60
Imai, H., He, J.-H., Nakashima, J., Ukita, N., Deguchi, S., & Koning, N. 2009, PASJ, 61, 1365
Imai, H., Kurayama, T., Honma, M., & Miyaji, T. 2013b, PASJ, 65, 28 (Paper II)
Imai, H., Nakashima, J., Diamond, P. J., Miyazaki, A., & Deguchi, S. 2005, ApJL, 622, L125
Imai, H., Obara, K., Diamond, P. J., Omodaka, T., & Sasao, T. 2002, Natur, 417, 829
Imai, H., Sahai, R., & Morris, M. 2007, ApJ, 669, 424
Lewis, B. M. 2001, Natur, 560, 400
te Lintel Hekkert, P., Versteege-Hensel, H. A., Habing, H. J., & Wiertz, M. 1989, A&AS, 78, 399
Miranda, L. F., Gómez, Y., Anglada, G., & Torrelles, J. M. 2001, Natur, 414, 284
Sahai, R. 2004, in ASP Conf. Ser. 313, Asymmetrical Planetary Nebulae III: Winds, Structure and the Thunderbird, ed. M. Meixner et al. (San Francisco, CA: ASP), 141
Sahai, R., Morris, M., Sánchez Contreras, C., & Claussen, M. 2007, AJ, 134, 2200
Sahai, R., & Trauger, J. 1998, AJ, 116, 1357
Sevenster, M. N., van Langevelde, H. J., Moody, R. A., et al. 2001, A&A, 366, 481
Suárez, O., Francisco Gómez, J., Bendjoya, P., et al. 2012, in IAU Symp. 287, Cosmic Masers—from OH to H_0, ed. R. S. Booth, E. M. L. Humphreys, & W. H. T. Vlemmings (Cambridge: Cambridge Univ. Press), 230
Suárez, O., Gómez, J. F., Miranda, L. F., et al. 2009, A&A, 505, 217
Tafoya, D., Imai, H., Gomez, Y., et al. 2011, PASJ, 63, 71
Vinković, D., Blöcker, T., Hofmann, K.-H., & Elitzur, M. 2004, MNRAS, 352, 852
Vlemmings, W. H. T., Diamond, P. J., & Imai, H. 2006, Natur, 440, 58
Vlemmings, W. H. T., & van Langevelde, H. J. 2007, A&A, 472, 547
Yung, B. H. K., Nakashima, J., Imai, H., et al. 2011, ApJ, 741, 94 (Paper I)